Macromolecules

pubs.acs.org/Macromolecules Article

Polymer Microstructure Directs the Solvent-Selective Swelling Response of Polymer Brushes

Adam P. Humpal, Alexander Dhupar, Ram Prasad Sekar, Nancy S. Muyanja, Anuj Chauhan, and Ramya Kumar*

Cite This: Macromolecules 2025, 58, 9110−9121

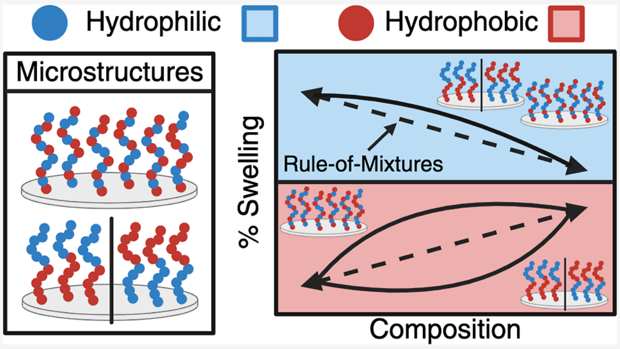

ABSTRACT: To exploit polymer brushes' solvent-responsive properties for applications in nanoparticle transport and sensing, we must elucidate how polymer composition and polymer microstructure shape brush swelling in varied solvent environments. We compared the solvent-selective response of block and statistical copolymer brushes of varied solvophobic-to-solvophilic ratios by measuring brush swelling in two solvents of varying polarity. We first copolymerized 2-(dimethylamino)ethyl methacrylate (DMA) and 2-(diisopropylamino)ethyl methacrylate (DiPA) and tuned DMA/DiPA ratios in block and statistical copolymer brushes. Then, we selectively quaternized DMA to enlarge solvophilicity differences between DMA and DiPA:water but not isopropanol is a good solvent for qDMA whereas DiPA exhibits the opposite solvation preference. In water, increasing DiPA incorporation depressed brush swelling for both block and statistical copolymer brushes. However, in isopropanol, swelling responses diverged; block copolymer brushes swelled between 9 and 37% less than compositionally equivalent statistical copolymer brushes. Additionally, we investigated the feasibility of deploying our polymer brushes in cell-interfacing applications by evaluating cytocompatibility. We established that the spatial distribution—and not just the relative abundance of solvophobic and solvophilic repeat units—governs polymer brushes' solvent responsivity.

■ INTRODUCTION

Polymer brushes, surface modifiers that impart desired interfacial properties to functional materials, have emerged as highly versatile surface engineering tools. For instance, polymer brushes have augmented the performance of nanocarriers for drug delivery,[1−4] membranes for water purification,[5−8] protein-resistant surfaces,[9−11] catalysts,[12−14] cell culture substrates,[15−18] and biosensors.[19−21] Chemists generally prefer "grafting from" approaches wherein they graft polymers from surface-immobilized initiator layers at grafting densities high enough that polymer end-to-end distances exceed the spacing between grafting sites.[22,23] Advances in surface characterization techniques and initiator immobilization methods have spurred rapid strides in decoding the physical behavior of polymer brushes.[24] In the last two decades, the expanded monomer scope and architectural diversity potentiated by surface-initiated atom transfer radical polymerization (SI-ATRP)[25] led chemists to investigate stimuli-responsive polymer brushes.[26] Stimuli-responsive polymer brushes undergo programmable conformational changes—swelling, collapse, or rearrangement—in response to environmental triggers such as temperature,[27,28] pH,[29] ionic strength,[30,31] or solvent properties.[32,33] Interestingly, many stimuli-responsive polymer brushes encode memory through their hysteretic behavior, further enriching their utility.[34−37]

Earlier work revealed how polymer composition, brush thickness, and grafting density direct the conformational evolution of thermoresponsive and pH-responsive brushes.[37−41] To minimize their free energy, solvent-responsive brushes adopt extended conformations in good solvents and collapsed conformations in poor solvents. We wish to frustrate this process by combining monomers with contrasting solvent preferences. Our long-term goal is to engineer surface modifiers based on polymer brushes encoding optimized spatial patterns and compositional ratios of solvophilic and solvophobic segments, such that brushes readily reconfigure their conformations in response to solvent environments. We refer to these brushes as solvent-responsive—those containing at least two monomers with

Received: June 22, 2025
Revised: August 19, 2025
Accepted: August 20, 2025
Published: August 24, 2025

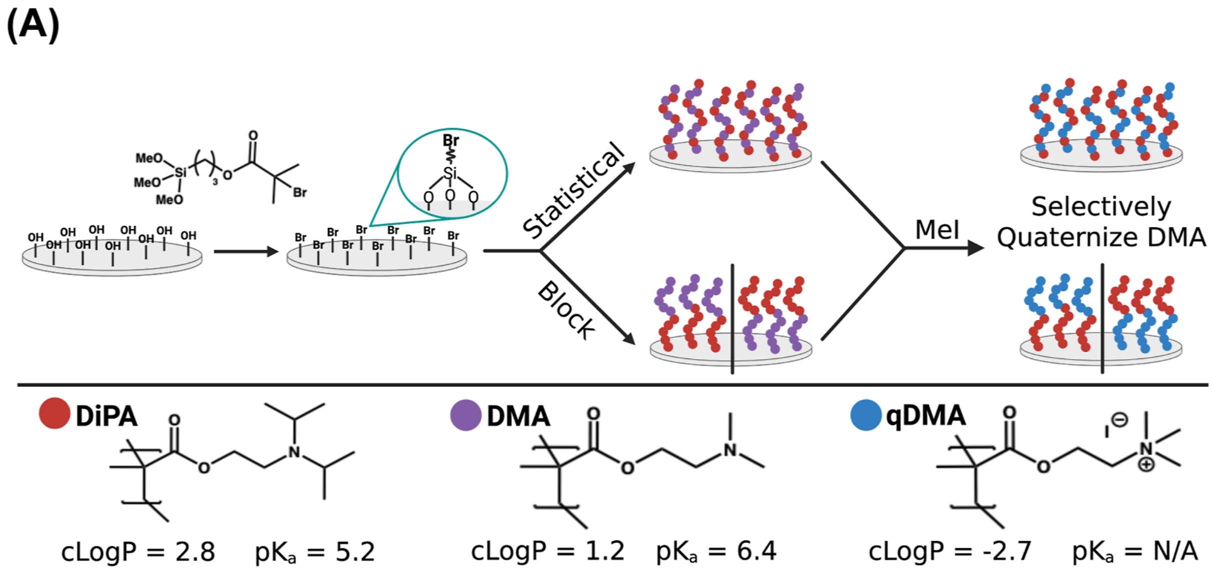

(B)

Sample ID	%DiPA [%]	Pre-Quaternization: Microstructure	h_{dry} [nm]	$\theta_{ses.}$ [°]	R_q [nm]	Post-Quaternization: Microstructure	h_{dry} [nm]	$\theta_{ses.}$ [°]	R_q [nm]
(q)DMA	0±0		23±0.2	58±0.5	1.35		31±0.1	55±0.5	1.15
DiPA	100±0		39±0.1	75±0.8	1.07		37±0.1	61±1.1	1.50
(q)S-32	32±1		28±0.1	59±0.7	1.43		34±0.1	56±1.5	1.10
(q)S-53	53±1		32±0.2	61±0.7	1.67		36±0.1	61±1.0	1.54
(q)S-64	64±5		35±0.1	62±0.6	1.63		37±0.0	56±1.2	1.71
(q)B1-18	18±1		44±0.1	55±1.2	1.29		56±0.1	57±2.7	1.28
(q)B1-43	43±0		31±0.1	56±0.4	1.92		39±0.3	59±2.3	1.86
(q)B1-82	82±1		28±0.1	66±0.5	1.81		29±0.1	55±0.7	1.10
(q)B2-87	87±2		49±4.9	71±0.9	2.63		47±3.9	63±0.8	1.18
(q)B2-72	72±2		36±1.7	74±0.2	2.83		39±0.1	59±0.9	1.19
(q)B2-45	45±2		25±0.7	72±2.0	2.79		30±0.1	64±0.7	1.02

Figure 1. Overview of polymer brush synthesis and characterization. (A) First, we grafted copolymer brushes comprising DMA and DiPA from ATRP initiator-functionalized substrates. Then, we quaternized DMA selectively to amplify hydrophilicity differences. (B) Polymer composition (% DiPA) was determined via X-ray photoelectron spectroscopy; dry brush thickness (h_{dry}) from ellipsometry; advancing contact angle ($\theta_{adv.}$) through contact angle goniometry, and roughness (R_q) via atomic force microscopy. Figure created with BioRender.

different solvent preferences—this terminology is based on the precedence set by Dong and Zhou.[42,43]

We foresee that our solvent-responsive brushes can be applied as microfluidic logic gates or cell culture substrates that dynamically respond to changes in media composition to tune cell adhesion.[44] Further, as surface modifiers, these solvent-responsive brushes can augment nanoparticle transport at solvent interfaces (e.g., lipid-water barriers in drug delivery).[45] We can track the conformational evolution of solvent-responsive brushes by monitoring changes in brush thickness and wettability in varied solvent environments. How should we distribute solvophilic and solvophobic repeat units in copolymer brushes to maximize their swelling response in contrasting solvent environments? To answer this, we reveal the mechanisms through which polymer composition and microstructure dictate the swelling responses of polymer brushes incorporating repeat units with varied solvent preferences. Our study is the first to systematically compare compositionally matched block and statistical copolymer brushes incorporating solvophilic and solvophobic groups and to elucidate the impact of block sequence on swelling response. We made important methodological contributions: overcoming synthetic challenges to obtain statistical copolymer brushes of mutually incompatible solvophobic and solvophilic monomers and developing XPS analysis methods to overcome surface enrichment phenomena (wherein hydrophobic segments are over-represented at brush−air interfaces).

Polymer microstructure has hitherto been a powerful design handle to tune the properties and performance of micelles, polyelectrolyte complexes, bottlebrushes, and other polymeric

https://doi.org/10.1021/acs.macromol.5c01659
Macromolecules 2025, 58, 9110−9121

materials.[46−49] Yet, we do not understand how microstructural contrasts between statistical, block, gradient copolymers, or mixed polymer brushes (chemically distinct homopolymers grafted from the same substrate) tune brush swelling or collapse in diverse solvent environments. Yuan and co-workers simulated conformational changes of pH responsive brushes and found that the spatial arrangement of ionizable repeat units dictates the pH responsivity.[50] Sanjuan and Tran compared microstructural effects of pH-dependent polyelectrolyte complexation in amphoteric brush systems which incorporate both polyacid and polybase segments.[51] For amphoteric brushes, the mechanism of brush collapse is distinct from solvophobic induced deswelling.[52] In contrast, we investigate solvophobic/solvophilic interactions that result in brush collapse/swelling.

Others have extended these results to thermoresponsive and solvent-responsive polymers.[53,54] Computational and experimental studies verified that binary "mixed" brushes consisting of hydrophobic and hydrophilic homopolymers readily switch conformations when removed from an aqueous environment and placed in an oil phase and vice versa.[55−58] Encouraged by these results, researchers grafted mixed brushes to stabilize ultrasmall nanoparticles such as quantum dots in both aqueous and apolar solvents.[59] Although binary mixed brushes are valuable model systems to validate predictions from simulations, synthetic challenges impede precise control over brush density, brush thickness, and the hydrophobic-to-hydrophilic ratio. These mixed brushes demand specialized approaches such as Y-shaped initiators,[60,61] initiator backfilling,[36] or codeposition of reversible addition−fragmentation chain transfer (RAFT) polymerization and ATRP initiators.[62,63]

Unlike mixed polymer brushes, we can tune the solvophobic-to-solvophilic ratio of block copolymer brushes merely by altering the block lengths. Zhao and Brittain showed that block copolymers incorporating polystyrene (PS) and methyl methacrylate (MMA) exhibited contrasting conformations in cyclohexane (a selective solvent for PS) and dichloromethane (a good solvent for both MMA and PS) with styrene and MMA repeat units dominating the surface in cyclohexane and dichloromethane, respectively.[64] Building on this work, Xu et al. mapped how block lengths and composition governed interfacial properties.[65] Above a critical block length, the top block dominates surface properties; below that critical length the ratio of block lengths of top and bottom blocks tune surface properties.[65] Further, we can access interesting properties merely by switching the block sequence; in AB-type diblock copolymer brushes, either A or B can be the top or bottom blocks, respectively.

Statistical copolymer brushes lack the long-range separation between solvophobic and solvophilic repeat units characteristic of block copolymer brushes. Yet recent studies have revealed that statistical copolymer brushes exhibit interesting stimuli-responsive properties. Ramezani Bajgiran et al. varied the spatial distribution of cationic and neutral repeat units in statistical copolymer brushes to tune polycation protonation degree and brush swelling.[37] Here, we ask a different question: how does the solvophobic-to-solvophilic ratio in statistical copolymer brushes modulate the swelling response in diverse solvents? What makes this question challenging to address is the difficulty of synthesizing statistical copolymer brushes in one-pot reactions where it would be near-impossible to dissolve monomers with contrasting solvent preferences. We overcome this synthetic difficulty by selecting a monomer pairing that is amenable to one-pot copolymerization and subsequent post-polymerization (Figure 1). Post-polymerization modification methods are commonly employed in the synthesis of brushes to overcome monomer−catalyst interactions or to enhance antifouling properties, however, such techniques are rarely applied to create contrasting solvent preferences.[66]

To map how microstructure and solvophobic-to-solvophilic ratio dictate swelling response in different solvents, we synthesized statistical and block copolymer brushes spanning a broad range of compositions (18−87% hydrophobic monomer). We address lacunae in previous work on solvent-responsive brushes, which predominantly employed contact angle goniometry or atomic force microscopy to monitor solvent-triggered conformational changes. These surface-sensitive techniques fail to probe the entire brush depth, failing to fully elucidate swelling mechanisms. Instead of merely inspecting surface-level changes in brush properties, we apply liquid cell in situ ellipsometry. Thus, we directly measured the swelling ratio—the change in brush thickness relative to dry thickness after equilibration in either solvent. Brush swelling was measured in two solvents—one that preferentially solvates hydrophilic units and another selective to the hydrophobic units. For the first time, we demonstrate that polymer brush microstructure modulates solvent responsivity. Contrasting behavior based on microstructure is most apparent at intermediate solvophobic-to-solvophilic brush compositions. These findings illuminate brush swelling mechanisms for statistical copolymer brushes, which has never been investigated before, and reveal how microstructure governs brush swelling.

■ RESULTS AND DISCUSSION

We reveal how polymer microstructure (block vs statistical) and solvophobic-to-solvophilic ratios shape the solvent responsivity of polymer brushes. Our work is the first to systematically compare the swelling behavior of compositionally equivalent block and statistical copolymer brushes. We first copolymerized 2-(dimethylamino)ethyl methacrylate (DMA) and 2-(diisopropylamino)ethyl methacrylate (DiPA) via SI-ATRP (Figure 1A). Our rationale for monomer selection was based on two factors. First, the water−octanol partition coefficients (*c*log *P*, a measure of hydrophobicity) of DiPA and DMA diverged widely, suggesting that they exhibit contrasting solvent preferences. Second, pairing DMA with DiPA permits independent control over the brush composition and thickness. We can readily synthesize block copolymer brushes incorporating DiPA and DMA via sequential SI-ATRP reactions; but statistical copolymer brushes present a greater challenge due to the difficulty of finding mutually compatible reaction solvents for DiPA and DMA. Although deprotonated DiPA (*c*log P = 2.8) is as hydrophobic as canonical hydrophobic monomers such as *n*-butyl methacrylate (*c*log P = 2.9), we preferred DiPA, as it readily undergoes ATRP in water−alcohol solvent mixtures. We successfully identified one-pot reaction conditions in which DiPA and DMA could be copolymerized with well-controlled SI-ATRP kinetics (Figure S1 in Supporting Information). We overcame this synthetic bottleneck that had earlier prevented researchers from obtaining insights into how the spatial arrangement of solvophilic and solvophobic repeat units impacted polymer brush conformational changes in different solvents.

https://doi.org/10.1021/acs.macromol.5c01659
Macromolecules 2025, 58, 9110−9121

To explore a greater range of hydrophilicity contrasts than what is possible with DiPA and DMA, we applied a postpolymerization quaternization reaction developed by Bütün et al.[67] We selectively quaternized tertiary amine groups in DMA—but not DiPA—to amplify hydrophilicity differences. Quaternized DMA (qDMA) remains ionized across all pH values; in contrast, the steric hindrance imposed by isopropyl groups effectively prevents the quaternization of DiPA. As a consequence of selective quaternization of DMA to qDMA, we went from 1.6 orders of magnitude difference in *c*log *P* between DMA and DiPA to 5.5 orders of magnitude difference in *c*log *P* between qDMA and DiPA (Figure 1A). In addition to enlarging hydrophobicity differences with DiPA, the conversion of DMA from a weak to strong polyelectrolyte introduces electrostatic interactions. Studying these interactions is outside the scope of our research since we emphasize solvophilic swelling interactions over electrostatic considerations. We direct readers to earlier reports on strong polyelectrolyte brushes.[68,69] Here, we map how swelling ratio varies with solvophobic-to-solvophilic ratio and microstructure, focusing on trends in swelling ratio rather than the absolute values of percent swelling itself.

We synthesized 21 (co)polymer brushes with systematically varied polymer microstructure and incorporation levels of DiPA (% DiPA). Statistical copolymer brushes (S brushes) varied in their DiPA content (32 to 64%) and were subsequently quaternized (qS brushes). Two sets of block copolymer brushes with varying block sequences—B1 wherein DiPA forms the bottom block and B2 where DiPA forms the top block—were also synthesized with DiPA incorporation levels varying between 18−82% and 45−87% respectively. B1 and B2 brushes were quaternized to yield qB1 and qB2 brushes, respectively. We extensively characterized differences in polymer brush composition, thickness, roughness, wettability, and swelling responses in water and isopropanol (Figure 1B). Our work identifies molecular design principles for designing polymer brushes with tailored solvent swelling responses.

We Varied the Relative Abundance and Spatial Distribution of Solvophobic and Solvophilic Repeat Units. We confirmed successful copolymer brush synthesis and quaternization via grazing angle Fourier-transformed infrared (FTIR) spectroscopy (which provides structural information) and X-ray photoelectron spectroscopy (which provides elemental composition). Further, dry brush thicknesses (obtained via spectroscopic ellipsometry in Figure 1B) were comparable across statistical copolymers (S) and the block copolymers (B1, B2), spanning a range between 25 and 40 nm. Figure S2 in the Supporting Information has details on reaction kinetics. In this thickness range, brush thickness variations will not confound interpretation of solvent swelling response.[70,71] We found it difficult to realize precise thickness targets for block copolymers due to the sluggish polymerization kinetics of the top block during the second SI-ATRP reaction. During the second SI-ATRP step in this sequential polymerization, the reaction rate from the bottom block proved to be highly sensitive to the block sequence. We obtained thickness values of 97−68% compared to virgin initiator controls for DiPA-on-DMA and 61−36% for DMA-on-DiPA (Figure S3 in the Supporting Information). We speculate that the DiPA brushes may not remain fully extended in the DMA reaction mass, limiting the speed at which active chain ends become accessible, depressing the measured thickness, and ultimately causing sluggish SI-ATRP kinetics for the top DMA block. Despite the slower top block kinetics, we do not see significant grafting density differences between samples, which is discussed in more detail later on in the results.

Quaternization increases brush thickness in a composition-dependent manner; DMA-rich brushes experienced a larger increase in dry thickness post-quaternization. For example, the thickness of DMA homopolymer brushes increased from 23 nm (pre-quaternization) to 31 nm (post-quaternization), a 35% increase in line with what we predict from molar volume differences between DMA and the bulkier qDMA (32%). Given the hygroscopic nature of strong polyelectrolytes like qDMA, atmospheric humidity may infiltrate brushes and trigger brush swelling even in a supposedly dry state.[72] As pointed out by Ko et al.,[73] obtaining the true dry brush thickness of polyelectrolyte films is challenging. Next, we analyzed brush roughness via atomic force microscopy (AFM), which revealed smooth films with low roughness values ($R_q < 2$ nm). DiPA-rich polymer brushes appeared more textured likely due to microphase separation (Figures S6 and S7 in the Supporting Information). The sessile water contact angle values are consistent with DiPA content—higher DiPA content yields higher contact angles. Further, microstucture also plays a role—DiPA-on-top block copolymer brushes yield higher contact angles. Discrepancies in these trends, especially once brushes are quaternized, are likely because of the brushes' propensity to rearrange and display low surface energy moieties on the surface resulting in more hydrophobic films.[74,75] Dynamic contact angle measurements revealed higher advancing contact angles, however, once the brushes are fully covered in water, they become highly hydrophilic (Figures S8−S10 in the Supporting Information). Hence, receding contact angles mostly fall below 30°. Both DiPA and (q)DMA contain hydrophilic and hydrophobic moieties, and while the pK_a value of DiPA brushes is 5.2. It has been shown that the periphery of a brush has a higher pK_a value than the bulk.[76] The pH of ultrapure water is around 6.3. Therefore, it is likely that surface DiPA units become protonated making the film appear hydrophilic despite DiPA being insoluble in water. These factors make the interpretation of contact angle data unreliable and necessitate swelling measurements via in situ ellipsometry.

We discuss representative FTIR spectra of quaternized statistical copolymer brushes, qS-32, qS-53, and qS-64 along with qDMA and DiPA homopolymer brushes here (Figure 2A). Additional FTIR spectra for the unquaternized statistical, quaternized and unquaternized block copolymers are provided in Figures S11−S15. Ester stretches were distinct at 1732 cm^{-1} (C═O) and 1153 cm^{-1} (C−O) (Figure 2A). We did not detect C═C stretches, confirming that unreacted monomers were completely removed during washing. Spectral differences between DiPA and qDMA can be observed in the C−C and C−H bands (2900−3000 cm^{-1}). Successful quaternization is evident in the 1670 cm^{-1}, 1481 cm^{-1}, and 955 cm^{-1} (Figure 2B) regions associated with the C−N stretches.[77] While FTIR cannot quantify DiPA incorporation, the gradual increase in the intensity of C−C and C−H suggests a transition from qDMA-rich (qS-32) to DiPA-rich (qS-64) statistical copolymers.

We also measured the refractive indices of polymer brushes via spectroscopic ellipsometry. In Figure 2C, the refractive index tracks changes in brush composition, permitting us to

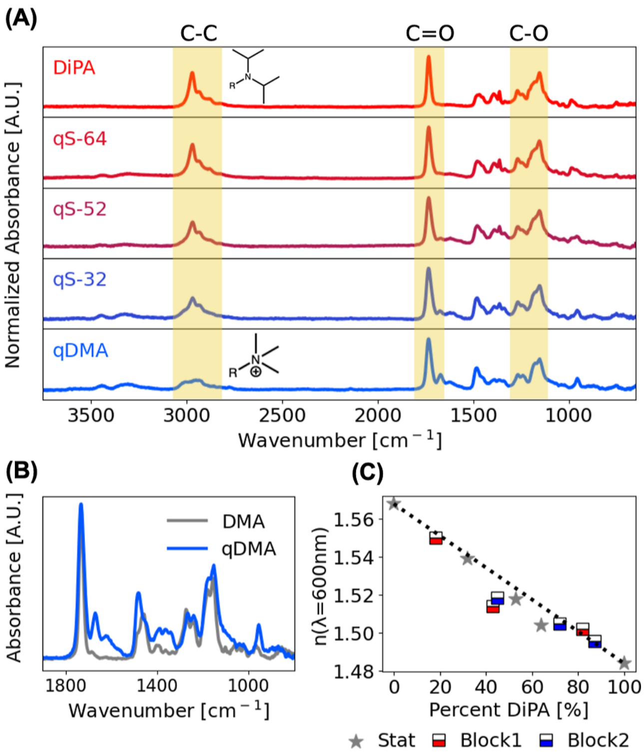

Figure 2. FTIR and refractive index measurements captured compositional ratios of DiPA and (q)DMA. (A) FTIR spectra of quaternized statistical (qS) copolymer brushes with key bands in regions characteristic of DiPA and quaternized DMA highlighted. (B) FTIR spectral differences between DMA (gray) and qDMA (blue) homopolymer brushes. (C) Refractive index (at λ = 600 nm) of quaternized brushes was determined via spectroscopic ellipsometry and a Cauchy fit. The refractive index was sensitive to brush composition, decreasing with DiPA incorporation, allowing us to verify FTIR trends.

monitor quaternization reactions. Both DiPA and DMA have very similar refractive indices ($n(\lambda$ = 600 nm) = 1.48). However, the refractive index of DMA increases sharply after quaternization ($n(\lambda$ = 600 nm) = 1.57 for qDMA). Hence, polymer brushes with higher refractive indices (close to 1.57) indicate qDMA-dominant brushes whereas brushes with lower refractive indices (close to 1.48) suggest DiPA-dominant brushes. We achieved quaternization efficiencies exceeding 80%, which we discuss below.

Although FTIR and refractive index measurements illuminated compositional differences, we additionally performed X-ray photoelectron spectroscopy (XPS) to quantify DiPA incorporation rigorously. DiPA and DMA homopolymers display similar elemental compositions since they differ merely in carbon content, which is not a reliable compositional metric due to adventitious carbon. Fortunately, XPS clearly discriminates between qDMA and DiPA in two ways: (1) iodide counterions associated with quaternized amines are visible (I_{3d}), (2) the N_{1s} peak splits into two based on the relative abundance of tertiary (399 eV) and quaternary (402 eV) amines, respectively.[78] We applied both of these approaches—iodine content and deconvolution of high resolution N_{1s} XPS spectra—to quantify qDMA content. We calculated the qDMA content from the first approach (iodine-to-nitrogen (I/N) ratio) in Figure 3, but we also estimated the qDMA content from high resolution nitrogen spectra (Figures S19−S22 in Supporting Information). The quaternization efficiency of CH_3I vapor treated DMA brushes was around 81% (Figure S5 in Supporting Information), consistent with earlier reports.[77,78] To obtain the quaternization efficiency, we employed a spin-coated film of 100% quaternized DMA (synthesized via RAFT in solution) as a reference sample in XPS. This reference sample was characterized via ^{1}H NMR to verify 100% quaternization (Figure S4 in the Supporting Information). We normalized the I/N ratio from the copolymer brushes to that obtained from qDMA under the same reaction conditions. This approach accounts for partially complete quaternization and ensures accurate quantification of % DiPA in statistical copolymer brushes. Block copolymer brushes necessitated a different approach since XPS cannot penetrate the entire depth of top and bottom blocks. Hence, instead of XPS, we transformed dry brush thickness measurements to molar ratios after determining the density of each block (see the Methods section and Page S8 in the Supporting Information for details).

Initially, XPS indicated far lower iodine content in quaternized statistical copolymer brushes compared to predicted values from refractive index measurements. We suspected that DiPA enriched brush surfaces to reduce the interfacial contact area between air (nonpolar) and the highly polar qDMA (Figure S17 in the Supporting Information). Given that the XPS probe depth is around 10 nm,[79] if qDMA gets displaced even by only a few nanometers below the surface by DiPA, this surface rearrangement would significantly skew the XPS data. If DiPA dominated the top 3 nm (which is the mean free path for C_{1s} electrons), DiPA would represent ~70% of the total photoelectrons collected. We confirmed our suspicion of DiPA surface enrichment via hard X-ray XPS analysis, which has a higher probe depth (Figure S16 in the Supporting Information). Further, to ensure that DiPA surface enrichment does not confound % DiPA estimates, we ablated the surface layer of polymer brushes through argon gas cluster ion sputtering. Interestingly, sputtering revealed a uniform layer of polymer brushes free of DiPA enrichment. Subsequently, we collected XPS spectra from freshly sputtered surfaces (Figure S18 in the Supporting Information). XPS spectra from sputtered surfaces yielded I/N ratios consistent with compositions predicted by refractive index trends (Figures S17−S21 in the Supporting Information). We present this detailed XPS analysis as a point of caution for future researchers studying copolymer films incorporating functional groups with dissimilar surface free energies. XPS affirmed that we obtained a wide range of DiPA incorporation levels for both block copolymer (DiPA on top or bottom) and statistical copolymer brushes. Next, we compared solvent responsivity as a function of solvophobic-to-solvophilic compositional ratios and brush microstructure.

Composition and Microstructure Govern the Solvent Responsivity of Copolymer Brushes. We assessed polymer brushes' swelling response in water and in isopropanol via liquid cell ellipsometry in situ. Water preferentially solvates qDMA (but not DiPA) whereas isopropanol solvates DiPA (but not qDMA). DiPA and qDMA repeat units exhibit contrasting solubility in water and isopropanol, making these two solvents appropriate to map the effects of microstructure and composition on solvent responsivity. We obtained swelling ratios by normalizing swollen brush thicknesses to their respective dry brush thicknesses.

https://doi.org/10.1021/acs.macromol.5c01659
Macromolecules 2025, 58, 9110−9121

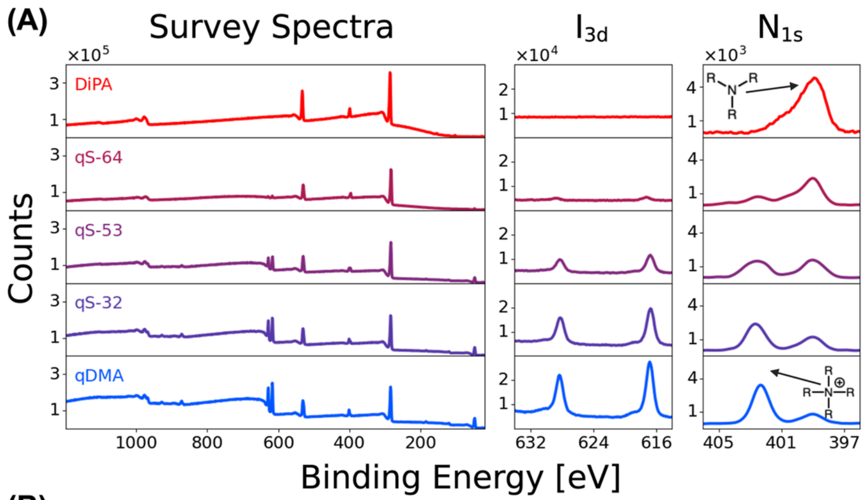

(B)

Sample ID	I_{3d} / N_{1s} Pre-Sputter	I_{3d} / N_{1s} Post-Sputter
DiPA	0.00 ± 0.00	-
S-32	0.02 ± 0.00	0.23 ± 0.02
S-53	0.18 ± 0.01	0.31 ± 0.00
S-64	0.35 ± 0.01	0.45 ± 0.01
qDMA	0.40 ± 0.05	0.65 ± 0.10

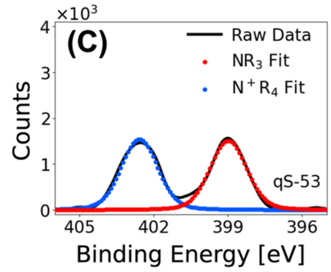

Figure 3. (A) XPS spectra of quaternized statistical brushes (unsputtered). I_{3d} and N_{1s} high resolution scans depict differences between DiPA and qDMA. (B) XPS analysis of polymer brush composition (sputtering overcomes DiPA surface enrichment effects). (C) Peak deconvolution of N_{1s} discriminates between tertiary and quaternary amines from DMA and qDMA (qS-53).

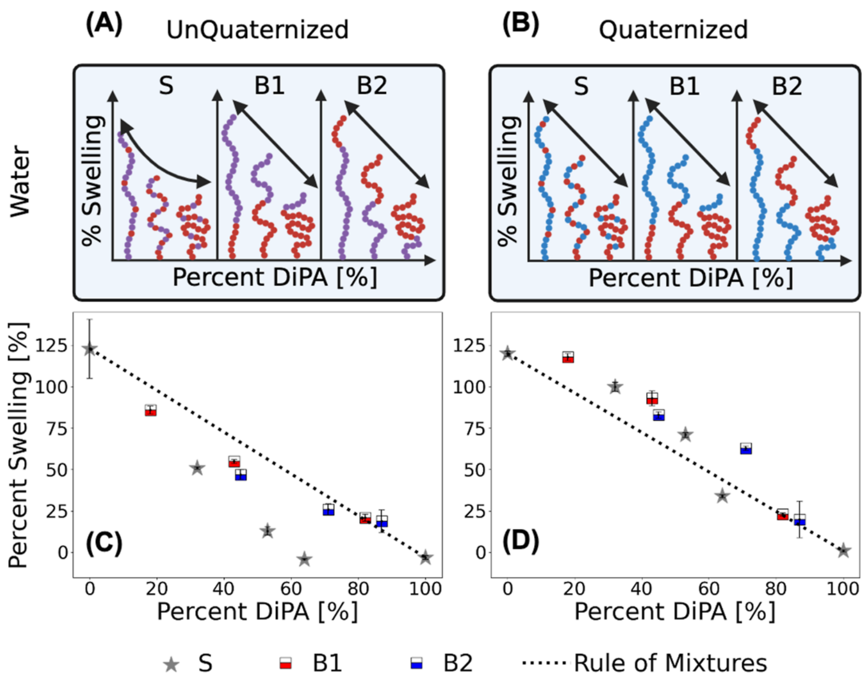

Figure 4. (A,B) Microstructure and composition dictate polymer brush swelling in water. Unquaternized block copolymer brushes follow "rule-of-mixtures" trends whereas unquaternized statistical brushes do not. Both sets of quaternized brushes exhibit linear trends irrespective of microstructure. Swollen brush thickness was normalized to dry brush thickness to obtain percent swelling. Swelling data was collected for both unquaternized (C) and quaternized (D) brushes via liquid cell ellipsometry. Figure created with BioRender.

The aqueous swelling ratios for unquaternized statistical copolymer brushes fall below linear "rule-of-mixtures" trend-lines, particulary at intermediate compositions (Figure 4C). In contrast, the aqueous swelling ratios of unquaternized block copolymer brushes decrease linearly with increasing DiPA (or decreasing DMA), largely conforming to "rule-of-mixtures" predictions. Interestingly, these differences between statistical and block microstructures vanish after quaternization

https://doi.org/10.1021/acs.macromol.5c01659
Macromolecules 2025, 58, 9110−9121

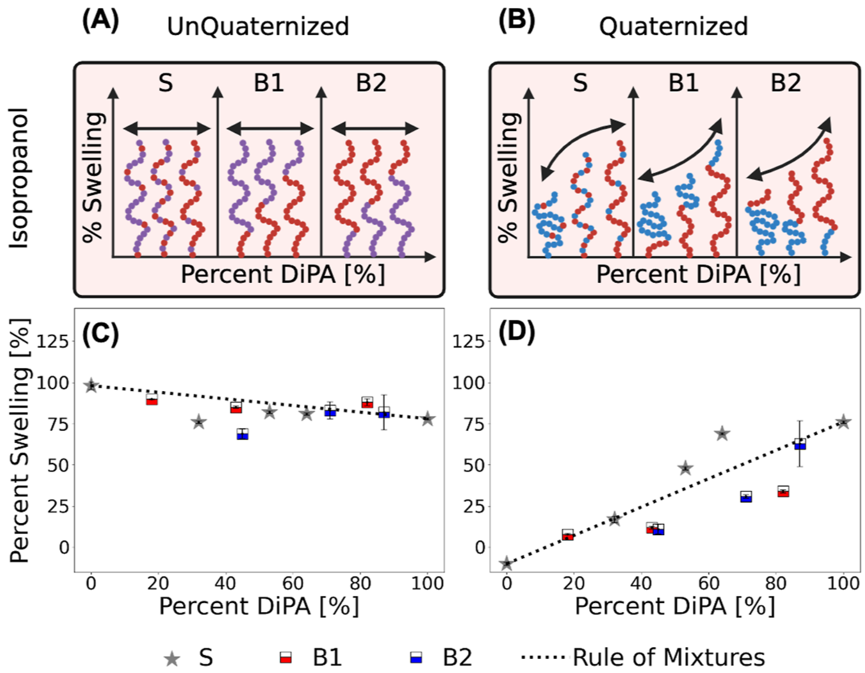

Figure 5. (A,B) Microstructure and composition dictate polymer brush swelling in isopropanol. Unquaternized brushes follow "equal swelling" trends where neither microstructure nor composition impact brush swelling in isopropanol. However, the percent swelling of quaternized brushes in isopropanol increases with DiPA content. Quaternized block copolymer brushes swell less that compositionally equivalent quaternized statistical copolymer brushes. Swollen brush thickness was normalized to dry brush thickness to obtain percent swelling. Swelling data was collected for both unquaternized (C) and quaternized (D) brushes via liquid cell ellipsometry. Figure created with BioRender.

(4(D))—the aqueous swelling ratios of both quaternized block and statistical copolymer brushes decrease linearly with increasing DiPA. closely following the "rule-of-mixtures" line.

We believe this deviation in swelling behavior for the unquaternized statistical copolymer brushes versus block copolymer brushes is related to the pK_a of DMA. The effective pK_a values of unquaternized DMA and DiPA homopolymer brushes fall around 6.4 and 5.2, respectively (Figure S23 in the Supporting Information). In unquaternized statistical copolymer brushes, where DMA is interspersed between DiPA, DMA protonation is suppressed to minimize unfavorable interactions between water and DMA's hydrophobic DiPA neighbors. This suppression of protonation ultimately lowers the effective pK_a of DMA and depresses the swelling response of unquaternized statistical copolymer brushes. Suppression of polycation protonation has previously been reported for micelles that incorporate hydrophobic units along with protonatable amines,[80] but not for substrate-tethered polymer brushes. It appears that copolymer brushes not only adopt pK_a values intermediate between DiPA and DMA (Figures S23–S25 in the Supporting Information) but also exhibit hydrophobicity-dependent hysteresis.

Next, we asked how DiPA incorporation and polymer microstructure affect brush swelling in isopropanol (Figure 5). For unquaternized brushes (Figure 5C), where isopropanol is a good solvent for both DMA and DiPA, both block and statistical copolymer brushes swell considerably (78–98%). Swelling ratios remained largely insensitive to DiPA incorporation and polymer microstructure. The slight decrease in swelling from DMA to DiPA is due to solvent quality differences. Although isopropanol is a good solvent for both DMA and DiPA, it is a slightly better solvent for DMA than DiPA. Within this "good solvent" swelling regime, we employed de Gennes swelling models to estimate grafting density.[81,82] We obtained grafting densities of 0.68 chains/nm^2 and 0.59 chains/nm^2 for DiPA and DMA homopolymer brushes, respectively (Page S26 in the Supporting Information), representing a densely grafted brush regime. Encouragingly, these values align with Qu et al.,[70] who employed the same initiator immobilization chemistry. Qu et al., who also studied DMA, reported very similar values of swelling for DMA in water as we measured in our experiment.[70] Further, we calculated the grafting density for the statistical and block copolymer brushes (Figure S26 in the Supporting Information) and see that there is little variation in grafting density across all samples. Sample-dependent differences in grafting density are most troublesome in block copolymers where ineffective preservation of initiator sites can lead to asymmetric grafting densities between the bottom and top block. Such a scenario would manifest itself as block copolymers swelling more than compositionally equivalent statistical copolymers. We do not observe these microstructural deviations for unquaternized brushes in isopropanol, confirming that we preserve initiators with high fidelity irrespective of block sequence.

Unquaternized copolymers, irrespective of composition and microstructure, swell between 78 and 98% in isopropanol. However, in quaternized qDMA homopolymers, isopropanol strips the hydration layers bound to qDMA segments, dehydrating brushes. Unlike in unquaternized brushes, microstructure dictated the swelling responses of quaternized brushes in isopropanol. Statistical copolymer brushes swell more than what is predicted by linear rule-of-mixtures trendlines whereas block copolymer brushes swell less than predicted, possibly due to differences in polymer–solvent interactions between statistical and block copolymer brushes. In quaternized statistical copolymer brushes, qDMA (which is poorly solvated by isopropanol) neighbors DiPA (which swells

https://doi.org/10.1021/acs.macromol.5c01659
Macromolecules 2025, 58, 9110–9121

in isopropanol), mitigating unfavorable interactions between qDMA and isopropanol. In contrast, qDMA repeat units self-segregate in block copolymer brushes to avoid isopropanol. Further, unsolvated segregated qDMA creates qDMA–DiPA interfaces that locally suppress DiPA swelling responses in isopropanol. Consequently, quaternized statistical copolymer brushes enjoy more favorable interactions with isopropanol than compositionally equivalent block copolymers, which leads to contrasting swelling responses.

We note that block sequence—whether DMA is on top of DiPA or vice versa—did not impact swelling. Initially, we expected the top block to impede solvent infiltration into the bottom block; similar phenomena have been reported for contact angle measurements.[65] Our initial hypothesis was that a sufficiently thick top DiPA block would prevent water from interacting with the hydrophilic qDMA underneath, thereby suppressing swelling. However, in our protocol, we equilibrate polymer brushes in water or isopropanol for nearly 12 h before liquid cell ellipsometry and hence we do not expect kinetic barriers to affect swelling responses. Additionally, we tried to elucidate block sequence effects via QCM-D instead of in situ ellipsometry. We reasoned that QCM-D will provide time-resolved measurements before brushes equilibrate in solvents. However, solvent switching (air to water, water to isopropanol, and isopropanol to water) dominated the signal, rendering the analysis infeasible (Figure S27 in the Supporting Information). Overall, we discovered that statistical and block copolymer brushes exhibit distinct swelling responses in water and isopropanol.

To further investigate the role of microstructure on polymer brush properties, we performed cytocompatibilty assays (Figures S28–S31 in the Supporting Information). We learned that our brushes support cell growth, despite bearing quaternary amine groups, and can be applied in biomedical contexts (e.g., sensing and drug delivery). However, we did not detect statistically significant differences in cell viability between any of the quaternized samples (block vs statistical vs DMA homopolymer brushes).

■ CONCLUSIONS

Toward our long-term goals of engineering solvent-responsive brushes for applications in microfluidics, cell culture surface engineering, and nanoparticle surface modification for transport across solvent interfaces, we identified polymer brush attributes governing swelling behavior in diverse solvents. We established that the spatial distribution—and not just the relative abundance—of solvophobic and solvophilic repeat units governs the solvent responsivity of polymer brushes. We synthesized a library of 21 statistical or block (co)polymer brushes with varied monomer incorporation levels and spatial arrangement of hydrophobic DiPA and hydrophilic (q)DMA repeat units. We exploited postpolymerization modification to selectively quaternize DMA groups, thereby amplifying hydrophilicity contrasts between DiPA and DMA. All 21 (co)polymer brushes exhibited comparable roughness and brush thicknesses whereas wettability varied with quaternization state and DiPA incorporation. FTIR spectroscopy and refractive index measurements confirmed that we achieved desired compositional trends. We quantified DiPA incorporation via XPS and performed sputtering to overcome surface enrichment of DiPA segments. In situ liquid cell ellipsometry captured brush swelling responses in water and isopropanol as a function of DiPA incorporation, DMA quaternization state, and polymer microstructure. In water, the swelling ratio decreased linearly with DiPA content for both block and statistical copolymers, whether quaternized or not. However, in isopropanol, quaternized statistical and block copolymer brushes diverged in their swelling behavior—DiPA-rich statistical copolymer brushes swelled far more than predicted by linear rule-of-mixtures trends and equivalent block copolymer brushes swelled far less than predicted in isopropanol. These microstructural differences were most evident at intermediate compositions. As the composition of the brush neared that of a homopolymer, rule-of-mixtures was followed regardless of microstructure. We quantified the swelling responses of well-defined polymer brushes with systematically engineered contrasts in the spatial arrangement and relative abundance of solvophobic and solvophilic repeat units. Future investigations will map connections between polymer microstructure and the kinetics of solvent infiltration and brush swelling via quartz crystal microbalance measurements. We will additionally elucidate the effects of grafting density and expand the scope of our investigation to mixed brushes. Our work identifies important design considerations for solvent-responsive polymer brushes, and opens up applications for these dynamic surface modifiers in various domains such as microfluidics, biomedical engineering, and nanoparticle transport at interfaces. Our study offers both fundamental insights and method development (e.g., XPS techniques that overcome surface enrichment phenomena, one-pot copolymerization of monomers with incompatible solvent preferences) that will be useful for researchers studying stimuli-responsive polymer brushes.

■ EXPERIMENTAL SECTION

Materials. Anhydrous toluene, triethylamine, 2,2′-bipyridyl, copper(II) bromide, copper(I) chloride, dopamine hydrochloride, α-bromoisobutyryl bromide (BiBB), and tris(hydroxymethyl)-aminomethane (Tris) were purchased from Sigma-Aldrich (St. Louis, MO) and used as received. 2-(Dimethylamino)ethyl methacrylate (DMA) and 2-(diisopropylamino)ethyl methacrylate (DiPA) were purchased from Sigma-aldrich and purified by passing through a basic alumia column. Methyl iodide, LC/MS grade water, and LC/MS grade isopropanol were obtained through Thermo Fisher (Waltham, MA). (3-trimethoxysilyl)propyl 2-bromo-2-methylpropionate was purchased through Gelest (Morrisville, PA). 11-Mercaptoundecyl 2-bromo-2-methylpropanoate was bought from ProChimia Surfaces (Poland). Silicon wafers (100 mm, B-doped, ⟨100⟩, SSP) were purchased from University Wafers (Boston, MA) and cut to 15 mm × 60 mm dimensions.

Methods. *Surface Functionalization.* Silicon wafers were cleaned with water, ethanol, and underwent UV/Ozone treatment for 15 min. Cleaned wafers were placed in glass Petri dishes followed by 60 mL of anhydrous toluene, 100 μL of triethylamine, and 60 μL of (3-trimethoxysilyl)propyl 2-bromo-2-methylpropionate.[70] The wafers were left to react for 18 h then thoroughly rinsed with ethanol, dried with air and stored in a clean environment. To prepare gold wafers, thermal evaporation deposited a 50 nm layer of gold on silicon wafers with a 5 nm titanium adhesion layer. UV/Ozone cleaned gold-coated wafers were immersed in a 2 mM 11-mercaptoundecyl 2-bromo-2-methylpropanoate in ethanol solution, placed on a shaker at 50 rpm, and allowed to react for 18 h.[83] Initiator-functionalized gold-coated wafers were sonicated in ethanol to remove free initiators and used immediately for SI-ATRP.

Synthesis of Copolymer Brushes. Copolymer brushes of DiPA and DMA were prepared via SI-ATRP from initiator-functionalized silicon or gold wafers. A full account of the procedure to synthesize the polymer brushes can be found in the Supporting Information, a general reaction is presented here for DMA homopolymer brushes. A

https://doi.org/10.1021/acs.macromol.5c01659
Macromolecules 2025, 58, 9110–9121

solution of 2,2′ bipyridyl (161.1 mg, 1.03 mmol), copper(II) bromide (8.4 mg, 37.5 μmol), DMA (3.93 g, 25 mmol), isopropanol (10.4 mL), and water (10.4 mL) was prepared in a 25 mL Schlenk flask and deoxygenated via three cycles of freeze−pump−thaw. Then copper(I) chloride (37.1 mg, 375 μ mol) was added under a blanket of nitrogen, followed by another cycle of freeze−pump−thaw. Upon dissolution of the copper(I) chloride the blue reaction mass turned brown. This reaction mass was sonicated for 5 min to dissolve catalysts and transferred to a deoxygenated glovebag. The glovebag was again degassed by three cycles of vacuum-nitrogen purging. The ATRP solution was transferred to vials with initiator-functionalized gold or silicon wafers and allowed to react for 90 min. For the statistical and homopolymer brushes, the reaction was stopped by removing the solution and thoroughly washing the substrates sequentially and repeatedly with isopropanol/water. To preserve the bromine-terminated end groups of the bottom block, the reaction was quenched with copper(II) bromide solution (500 mg Cu(II)Br_2, 1000 mg 2,2′ bipyridyl, 100 mL 70:30 isopropanol−water). All samples were sonicated and rinsed repeatedly with isopropanol to remove residual monomer.

Quaternization of Polymer Brushes. Polymer brushes were quaternized via vapor phase CH_3I treatment.[77] The samples were placed 5 mm above a 0.5 M solution of CH_3I in isopropanol. The reaction took place in a covered crystallization dish for 2 h. The samples were removed from the vapor chamber and rinsed with isopropanol and air-dried.

Ellipsometry. Dry brush thickness measurements were collected via an α-SE ellipsometer (J.A. Woollam) at an angle of 70 °across a wavelength range between 500 and 900 nm. Spectral data was analyzed with CompleteEASE using an optical model of silicon substrate with a 2 nm thick layer of native SiO_2. Polymer brushes were modeled as Cauchy layers. For the unquaternized brushes the parameters for the Cauchy model were fixed to A = 1.485, B = 0.004 μm^2. When quaternized, the refractive index n of the film increases. Hence, spectroscopic ellipsometry effectively captures quaternization degree. We obtained Cauchy parameters (A = 1.485−1.534, B = 0.004−0.0011 μm^2) by fitting experimental Δ and Ψ values across a wavelength range (500 to 900 nm) to Cauchy equations.

Liquid state ellipsometry was performed using an M-2000 ellipsometer (J.A. Woollam) equipped with a 5 mL liquid cell. Measurements were collected at an angle of 75°. LC−MS grade water and isopropanol were used as solvents for the swelling measurements. The substrates were equilibrated prior to measurement for 12 h and again allowed to equilibrate for 5 min after being loaded into the liquid cell. We applied an effective medium approximation (EMA) between polymer brushes and solvents to model the solvated film and obtain the swollen film thickness.[84]

Contact Angle Goniometry. Dynamic contact angle measurements were collected using a ThetaFlex Tensiometer (Biolin Scientific) equipped with a motorized syringe pump. Samples were cleaned with water, then isopropanol, followed by drying with clean air. A 3 μL water droplet was carefully deposited on the sample surface and 30-gauge needle was inserted into the drop. Water was added at a rate of 0.5 μL/s for 50 s (advancing contact angle) and removed at a rate of 0.25 μL/s for 105 s (receding contact angle). The advancing contact angle was determined by image analysis in OneAttension and performed in triplicate.

Fourier-Transformed Infrared Spectroscopy. FTIR spectra were gathered using a Nicolet 6700 spectrometer equipped with a smart SAGA attachment and an MCT detector. Polymers grafted from the gold-coated wafers yielded the best quality spectra with 64 scans per sample at a resolution of 4 cm^{-1}. Data analysis was performed in OMNIC software.

X-ray Photoelectron Spectroscopy. Chemical composition of the statistical copolymer brushes was determined using a Kratos Axis Supra$^+$ X-ray photoelectron spectrometer equipped with a monochromatic Al Kα source and Ar_n^+ gas cluster sputtering gun. Survey spectra were collected with a pass energy of 160 eV and a step of 1 eV. High-resolution scans of the C_{1s}, N_{1s}, and I_{3d} peaks were collected with a pass energy of 20 eV and a step size of 0.1 eV. Spectra were calibrated the binding energy of C−C, C−H peaks at 285 eV. Analysis was performed in CasaXPS.

Compositional Calculation for Block Copolymer Brushes. The mole fraction of DiPA to DMA for the block copolymers was determined from the thicknesses obtained by ellipsometry. Ellipsometry was performed first after synthesizing the bottom block and then repeated after synthesizing the top block. The thickness difference told us how thick the top block was. Once we estimated the thickness of the DiPA and DMA blocks, we converted these values to volume fractions. Then, we obtained DiPA and DMA mole fractions via eq 1.

$$M_1 = \frac{\frac{t_1}{V_{m,1}}}{\frac{t_1}{V_{m,1}} + \frac{t_2}{V_{m,2}}} \tag{1}$$

where M_1 is the mole fraction of DiPA, t_1 and t_2 are the thicknesses of DMA and DiPA, respectively, and $V_{m,1}$ and $V_{m,2}$ are the molar volumes of DiPA and DMA, respectively. The molar volume can be estimated from the monomer density and the molar mass. The density of DMA was reported as 0.93 g/cm^3,[73] therefore, given the molar mass of one repeat unit (157 g/mol) the molar volume is 169 cm^3/mol. The density of DiPA (213 g/mol) was determined from gas pycnometry to be 1.11 g/cm^3 (more information provided in Page S25 in the Supporting Information) leading to a molar volume of 192 cm^3/mol.

Atomic Force Microscopy. Topographic mapping and roughness analysis was performed using an atomic force microscope (Digital Instruments) in tapping mode with a 42 N/m silicon tip. The scan area was 5 μm × 5 μm with 512 data points per scan line. The scans were processed in Nano Scope V6 to determine the R_q roughness.

Functionalization of Polystyrene Substrates with Polydopamine-Based ATRP Initiators. For evaluating cell viability, polystyrene 24-well cell culture plates were coated with BiBB-functionalized-dopamine after modifying the procedure outlined by Zhu and Edmondson[85] Briefly, 379 mg (2.0 mmol) dopamine hydrochloride was dried under vacuum for 30 min in a 25 mL Schlenk flask. Anhydrous DMF (20 mL) was transferred to the flask under nitrogen. After complete dissolution of dopamine, 139 μL (1.0 mmol) triethylamine was added under nitrogen. Then 124 μL (1.0 mmol) BiBB was slowly injected into the flask under nitrogen. The solution was allowed to react for 4 h under nitrogen then diluted in 100 mL of Tris buffer. To make Tris buffer, 485 mg Tris base was dissolved in 100 mL water. One mL of the reaction mass was added to each well followed by 0.2 mL of sodium metaperiodate solution (898 mg in 10 mL of water). The reaction proceeded for 30 min. Then the reaction mass was removed and well plates thoroughly and repeatedly washed with water.

After confirming the formation of polydopamine-based SI-ATRP initiator coatings via FTIR spectroscopy, we performed copolymer brush synthesis from initiator-functionalized well plates according to the above procedures for cytocompatibility testing.

Cell Culture and Comparison of Cell Viability Across Polymer Brushes. Human embryonic kidney cells (HEK293) were procured from the American Type Culture Collection (ATCC), USA. HEK293 cells were grown in T-75 tissue culture flasks using DMEM with 10% fetal bovine serum (FBS) and 1% antibiotic−antimycotic solution and incubated at 37 °C/5% CO_2 in a humidified atmosphere. The cell culture media was changed every 2−3 days until the cells reached 80% confluence.

Polymer brush grafted 24-well plates were sterilized with 70% ethanol and air-dried for 2 h. The plates were subsequently washed with PBS (3×) and UV sterilized for 24 h. Following sterilization, the well plates were conditioned with complete DMEM medium for 24 h. The medium was then removed and 50,000 cells per well were seeded in 24-well polystyrene plates (untreated or polymer grafted). Cell-seeded well plates were incubated for 48 h at 37 °C and 5% CO_2. Cell culture media was replaced with fresh media at 24 h. After 48 h, the morphology of the cells was examined using an optical microscope

https://doi.org/10.1021/acs.macromol.5c01659
Macromolecules 2025, 58, 9110−9121

[Invitrogen EVOS XL Core Imaging System; Model: AMEX1000R] using a 10× objective lens with 0.25 NA/7.45 WD.

To evaluate the cell viability on polymer-grafted well plates, a CCK 8 cell viability assay was performed after 48 h of incubation. The cell culture media was replaced with Fluorobrite-DMEM media supplemented with CCK-8 solution (diluted according to manufacturer specifications). Cells were incubated in CCK-8-containing media for 4 h at 37 °C/5% CO_2. After 4 h of incubation, the supernatant media was transferred into 96-well plates, and absorbance was measured at 460 nm using a microplate reader (Synergy H1, BioTek, Winooski, VT, USA). The background of the CCK-8 solution was subtracted and the absorbance values were normalized to those of the untreated cells.

The number of viable cells was additionally quantified using flow cytometry. After the CCK-8 assay was performed, the cells were trypsinized, centrifuged at 1000 rpm for 5 min, and pellets were washed with PBS. The cells were stained with Calcein Red viability dye (400 nM) in PBS for 30 min at 23 °C. The cells were transferred to flow cytometry tubes (5 mL), and viable cell counts were quantified using flow cytometry (Cytek Northern Lights, California, USA).

ASSOCIATED CONTENT

Supporting Information

The Supporting Information is available free of charge at https://pubs.acs.org/doi/10.1021/acs.macromol.5c01659.

> Details pertaining to the reaction conditions of the brushes and additional characterization techniques, including FTIR, AFM, contact angle, XPS, pK_a determination, QCM-D data, micrographs of cells (PDF)

AUTHOR INFORMATION

Corresponding Author

Ramya Kumar − *Chemical and Biological Engineering, Materials Science, and Quantitative Biosciences and Engineering, Colorado School of Mines, Golden, Colorado 80401, United States;* orcid.org/0000-0002-8725-0023; Email: ramyakumar@mines.edu

Authors

Adam P. Humpal − *Materials Science, Colorado School of Mines, Golden, Colorado 80401, United States;* orcid.org/0009-0002-0777-5207

Alexander Dhupar − *Quantitative Biosciences and Engineering, Colorado School of Mines, Golden, Colorado 80401, United States*

Ram Prasad Sekar − *Chemical and Biological Engineering, Colorado School of Mines, Golden, Colorado 80401, United States;* orcid.org/0000-0003-3890-6230

Nancy S. Muyanja − *Michigan Center for Materials Characterization, University of Michigan, Ann Arbor, Michigan 48109, United States*

Anuj Chauhan − *Chemical and Biological Engineering, Colorado School of Mines, Golden, Colorado 80401, United States*

Complete contact information is available at: https://pubs.acs.org/10.1021/acs.macromol.5c01659

Notes

The authors declare no competing financial interest.

ACKNOWLEDGMENTS

Research reported in this publication was supported by the National Institute of Biomedical Imaging and Bioengineering of the National Institutes of Health under award number 1 R21 EB034464-01. Authors are grateful to Prof. Kevin Cash and his group for access to a plate reader. Some of the work was performed in following core facility, which is a part of Colorado School of Mines' Shared Instrumentation Facility (Optical and Electrical Characterization: RRID: SCR022047).The authors acknowledge the financial support of the University of Michigan College of Engineering and technical support from the Michigan Center for Materials Characterization for XPS measurements. Some figures in this work were created with BioRender. The authors do not have any conflicts of interest to disclose.

REFERENCES

(1) Li, D.; Sharili, A. S.; Connelly, J.; Gautrot, J. E. Highly Stable RNA Capture by Dense Cationic Polymer Brushes for the Design of Cytocompatible, Serum-Stable SiRNA Delivery Vectors. *Biomacromolecules* **2018**, *19*, 606−615.

(2) Liu, J.; Liu, Z.; Luo, X.; Zong, X.; Liu, J. RAFT Controlled Synthesis of Biodegradable Polymer Brushes on Graphene for DNA Binding and Release. *Macromol. Chem. Phys.* **2013**, *214*, 2266−2275.

(3) Zhai, Y.; Wu, L.; Gao, J.; Zhou, J.; Du, L.; Fu, X.; Gao, Y.; Zhang, T.; Zhang, M.; Lu, W.; Wu, Y. ROS-sensitive selenium-containing cationic brush polymer with potent gene transfection efficiency and biocompatibility. *J. Appl. Polym. Sci.* **2024**, *141*, No. e55199.

(4) Li, D.; Xu, L.; Wang, J.; Gautrot, J. E. Responsive Polymer Brush Design and Emerging Applications for Nanotheranostics. *Adv. Healthcare Mater.* **2021**, *10*, 2000953.

(5) Hu, J.; Li, M.; Wang, L.; Zhang, X. Polymer brush-modified graphene oxide membrane with excellent structural stability for effective fractionation of textile wastewater. *J. Membr. Sci.* **2021**, *618*, 118698.

(6) Ramesh, P.; Sorci, M.; Sengupta, B.; Karla, S.; Hao, Z.; Yu, M.; Kilduff, J.; Belfort, G. Highly tunable structure-by-design polymer brush membranes for organic solvent nanofiltration. *J. Membr. Sci.* **2023**, *678*, 121656.

(7) Bruening, M. L.; Dotzauer, D. M.; Jain, P.; Ouyang, L.; Baker, G. L. Creation of Functional Membranes Using Polyelectrolyte Multilayers and Polymer Brushes. *Langmuir* **2008**, *24*, 7663−7673.

(8) Nie, C.; Ma, L.; Xia, Y.; He, C.; Deng, J.; Wang, L.; Cheng, C.; Sun, S.; Zhao, C. Novel heparin-mimicking polymer brush grafted carbon nanotube/PES composite membranes for safe and efficient blood purification. *J. Membr. Sci.* **2015**, *475*, 455−468.

(9) Wei, T.; Tang, Z.; Yu, Q.; Chen, H. Smart Antibacterial Surfaces with Switchable Bacteria-Killing and Bacteria-Releasing Capabilities. *ACS Appl. Mater. Interfaces* **2017**, *9*, 37511−37523.

(10) Burmeister, N.; Zorn, E.; Preuss, L.; Timm, D.; Scharnagl, N.; Rohnke, M.; Wicha, S. G.; Streit, W. R.; Maison, W. Low-Fouling and Antibacterial Polymer Brushes via Surface-Initiated Polymerization of a Mixed Zwitterionic and Cationic Monomer. *Langmuir* **2023**, *39*, 17959−17971.

(11) Xu, G.; Liu, P.; Pranantyo, D.; Xu, L.; Neoh, K.-G.; Kang, E.-T. Antifouling and Antimicrobial Coatings from Zwitterionic and Cationic Binary Polymer Brushes Assembled via "Click" Reactions. *Ind. Eng. Chem. Res.* **2017**, *56*, 14479−14488.

(12) Pham Truong, T. N.; Randriamahazaka, H.; Ghilane, J. Polymer Brushes Ionic Liquid as a Catalyst for Oxygen Reduction and Oxygen Evolution Reactions. *ACS Catal.* **2018**, *8*, 869−875.

(13) Fernandes, A. E.; Ye, Q.; Collard, L.; Le Duff, C.; d'Haese, C.; Deumer, G.; Haufroid, V.; Nysten, B.; Riant, O.; Jonas, A. M. Effects of Thickness and Grafting Density on the Activity of Polymer-Brush-Immobilized Tris(triazolyl) Copper(I) Catalysts. *ChemCatChem* **2015**, *7*, 856−864.

(14) Xu, F. J.; Cai, Q. J.; Li, Y. L.; Kang, E. T.; Neoh, K. G. Covalent Immobilization of Glucose Oxidase on Well-Defined Poly(glycidyl methacrylate)-Si(111) Hybrids from Surface-Initiated Atom-Transfer Radical Polymerization. *Biomacromolecules* **2005**, *6*, 1012−1020.

(15) Psarra, E.; Foster, E.; König, U.; You, J.; Ueda, Y.; Eichhorn, K.-J.; Müller, M.; Stamm, M.; Revzin, A.; Uhlmann, P. Growth Factor-Bearing Polymer Brushes - Versatile Bioactive Substrates Influencing Cell Response. *Biomacromolecules* **2015**, *16*, 3530−3542.

(16) Górka-Kumik, W.; Garbacz, P.; Lachowicz, D.; Dąbczyński, P.; Zapotoczny, S.; Szuwarzyński, M. Tailoring cellular microenvironments using scaffolds based on magnetically-responsive polymer brushes. *J. Mater. Chem. B* **2020**, *8*, 10172−10181.

(17) Lishchynskyi, O.; Tymetska, S.; Shymborska, Y.; Raczkowska, J.; AwsiukSkirtachKorolkoChebotar, K. A. G. S. A.; Budkowski, A.; Stetsyshyn, Y.; Chebotar, A.; Budkowski, A.; Stetsyshyn, Y. Temperature-responsive properties of pH-sensitive poly(methacrylic acid)-grafted brush coatings with controlled wettability for cell culture. *J. Mater. Chem. B* **2025**, *13*, 3618−3632.

(18) Qian, X.; Villa-Diaz, L. G.; Kumar, R.; Lahann, J.; Krebsbach, P. H. Enhancement of the propagation of human embryonic stem cells by modifications in the gel architecture of PMEDSAH polymer coatings. *Biomaterials* **2014**, *35*, 9581−9590.

(19) Forinová, M.; Pilipenco, A.; Víšová, I.; Lynn, N. S. J.; Dostálek, J.; Mašková, H.; Hönig, V.; Palus, M.; Selinger, M.; Kočová, P.; et al. Functionalized Terpolymer-Brush-Based Biointerface with Improved Antifouling Properties for Ultra-Sensitive Direct Detection of Virus in Crude Clinical Samples. *ACS Appl. Mater. Interfaces* **2021**, *13*, 60612−60624.

(20) Degirmenci, A.; Yeter Bas, G.; Sanyal, R.; Sanyal, A. "Clickable" Polymer Brush Interfaces: Tailoring Monovalent to Multivalent Ligand Display for Protein Immobilization and Sensing. *Bioconjugate Chem.* **2022**, *33*, 1672−1684.

(21) Marquez, D. T.; Chawich, J.; Hassen, W. M.; Moumanis, K.; DeRosa, M. C.; Dubowski, J. J. Polymer Brush−GaAs Interface and Its Use as an Antibody-Compatible Platform for Biosensing. *ACS Omega* **2021**, *6*, 7286−7295.

(22) Azzaroni, O. Polymer brushes here, there, and everywhere: Recent advances in their practical applications and emerging opportunities in multiple research fields. *J. Polym. Sci., Part A: Polym. Chem.* **2012**, *50*, 3225−3258.

(23) Stuart, M. A. C.; Huck, W. T. S.; Genzer, J.; Müller, M.; Ober, C.; Stamm, M.; Sukhorukov, G. B.; Szleifer, I.; Tsukruk, V. V.; Urban, M.; Winnik, F.; Zauscher, S.; Luzinov, I.; Minko, S. Emerging applications of stimuli-responsive polymer materials. *Nat. Mater.* **2010**, *9*, 101−113.

(24) Zoppe, J. O.; Ataman, N. C.; Mocny, P.; Wang, J.; Moraes, J.; Klok, H.-A. Surface-Initiated Controlled Radical Polymerization: State-of-the-Art, Opportunities, and Challenges in Surface and Interface Engineering with Polymer Brushes. *Chem. Rev.* **2017**, *117*, 1105−1318.

(25) Yan, J.; Bockstaller, M. R.; Matyjaszewski, K. Brush-modified materials: Control of molecular architecture, assembly behavior, properties and applications. *Prog. Polym. Sci.* **2020**, *100*, 101180.

(26) Lee, H.-i.; Pietrasik, J.; Sheiko, S. S.; Matyjaszewski, K. Stimuli-responsive molecular brushes. *Prog. Polym. Sci.* **2010**, *35*, 24−44.

(27) Stetsyshyn, Y.; Raczkowska, J.; Harhay, K.; Gajos, K.; Melnyk, Y.; Dąbczyński, P.; Shevtsova, T.; Budkowski, A. Temperature-responsive and multi-responsive grafted polymer brushes with transitions based on critical solution temperature: synthesis, properties, and applications. *Colloid Polym. Sci.* **2021**, *299*, 363−383.

(28) Nastyshyn, S.; Stetsyshyn, Y.; Raczkowska, J.; Nastishin, Y.; Melnyk, Y.; Panchenko, Y.; Budkowski, A. Temperature-Responsive Polymer Brush Coatings for Advanced Biomedical Applications. *Polymers* **2022**, *14*, 4245.

(29) Li, S.; Guo, Z.; Zhang, H.; Li, X.; Li, W.; Liu, P.; Ren, Y.; Li, X. ABC Triblock Copolymers Antibacterial Materials Consisting of Fluoropolymer and Polyethylene Glycol Antifouling Block and Quaternary Ammonium Salt Sterilization Block. *ACS Appl. Bio Mater.* **2021**, *4*, 3166−3177.

(30) Xiao, S.; Ren, B.; Huang, L.; Shen, M.; Zhang, Y.; Zhong, M.; Yang, J.; Zheng, J. Salt-responsive zwitterionic polymer brushes with anti-polyelectrolyte property. *Curr. Opin. Chem. Eng.* **2018**, *19*, 86−93.

(31) Kim, D.; Hayashi, S.; Matsuoka, H.; Saruwatari, Y. Effect of Hydrophobicity and Salt on the Temperature Responsiveness of Polymeric Micelles Consisting of Hydrophobic and Sulfobetaine Chains. *Langmuir* **2023**, *39*, 1444−1455.

(32) Liu, Y.; Liu, Y.; Wu, Y.; Zhou, F. Tuning Surface Functions by Hydrophilic/Hydrophobic Polymer Brushes. *ACS Nano* **2025**, *19*, 11576−11603.

(33) Li, X.; Wang, Y.; Zhang, P. Theoretical investigation on the conformation of polymer brushes in mixtures of binary solvents. *J. Chem. Phys.* **2025**, *162*, 194903.

(34) Hollingsworth, N.; Larson, R. G. Hysteretic Swelling/Deswelling of Polyelectrolyte Brushes and Bilayer Films in Response to Changes in pH and Salt Concentration. *Polymers* **2021**, *13*, 812.

(35) Yadav, V.; Harkin, A. V.; Robertson, M. L.; Conrad, C. Hysteretic memory in pH-response of water contact angle on poly(acrylic acid) brushes. *Soft Matter* **2016**, *12*, 3589−3599.

(36) Ionov, L.; Minko, S. Mixed Polymer Brushes with Locking Switching. *ACS Appl. Mater. Interfaces* **2012**, *4*, 483−489.

(37) Ramezani Bajgiran, S.; Safi Samghabadi, F.; Li, S.; Conrad, J. C.; Marciel, A. B. Effects of the Ionizable Monomer Fraction on the Swelling Behavior of Weak Polyelectrolyte Brushes. *Macromolecules* **2023**, *56*, 9218−9228.

(38) Lego, B.; Skene, W. G.; Giasson, S. Swelling Study of Responsive Polyelectrolyte Brushes Grafted from Mica Substrates: Effect of pH, Salt, and Grafting Density. *Macromolecules* **2010**, *43*, 4384−4393.

(39) Bittrich, E.; Burkert, S.; Müller, M.; Eichhorn, K.-J.; Stamm, M.; Uhlmann, P. Temperature-Sensitive Swelling of Poly(N-isopropylacrylamide) Brushes with Low Molecular Weight and Grafting Density. *Langmuir* **2012**, *28*, 3439−3448.

(40) Hollingsworth, N. R.; Wilkanowicz, S. I.; Larson, R. G. Salt- and pH-induced swelling of a poly(acrylic acid) brush via quartz crystal microbalance w/dissipation (QCM-D). *Soft Matter* **2019**, *15*, 7838−7851.

(41) Johnson, E. C.; Willott, J. D.; de Vos, W. M.; Wanless, E. J.; Webber, G. B. Interplay of Composition, pH, and Temperature on the Conformation of Multi-stimulus-responsive Copolymer Brushes: Comparison of Experiment and Theory. *Langmuir* **2020**, *36*, 5765−5777.

(42) Dong, J.; Zhou, J. Solvent-Responsive Behavior of Polymer-Brush-Modified Amphiphilic Gold Nanoparticles. *Macromol. Theory Simul.* **2013**, *22*, 174−186.

(43) Xu, Y.; Chen, X.; Han, X.; Xu, S.; Liu, H.; Hu, Y. Lock/Unlock Mechanism of Solvent-Responsive Binary Polymer Brushes: Density Functional Theory Approach. *Langmuir* **2013**, *29*, 4988−4997.

(44) Espinosa-Marzal, R. M.; Nalam, P. C.; Bolisetty, S.; Spencer, N. D. Impact of solvation on equilibrium conformation of polymer brushes in solvent mixtures. *Soft Matter* **2013**, *9*, 4045−4057.

(45) Lin, Y.; Skaff, H.; Emrick, T.; Dinsmore, A. D.; Russell, T. P. Nanoparticle Assembly and Transport at Liquid-Liquid Interfaces. *Science* **2003**, *299*, 226−229.

(46) Faisal, K. S.; Clulow, A. J.; MacWilliams, S. V.; Gillam, T. A.; Austin, A.; Krasowska, M.; Blencowe, A. Microstructure—Thermal Property Relationships of Poly (Ethylene Glycol-b-Caprolactone) Copolymers and Their Micelles. *Polymers* **2022**, *14*, 4365.

(47) Chang, L.-W.; Lytle, T. K.; Radhakrishna, M.; Madinya, J. J.; Vélez, J.; Sing, C. E.; Perry, S. L. Sequence and entropy-based control of complex coacervates. *Nat. Commun.* **2017**, *8*, 1273.

(48) Jiang, L.; Nykypanchuk, D.; Pastore, V. J.; Rzayev, J. Morphological Behavior of Compositionally Gradient Polystyrene−Polylactide Bottlebrush Copolymers. *Macromolecules* **2019**, *52*, 8217−8226.

(49) Yang, C.; Wu, K. B.; Deng, Y.; Yuan, J.; Niu, J. Geared Toward Applications: A Perspective on Functional Sequence-Controlled Polymers. *ACS Macro Lett.* **2021**, *10*, 243−257.

(50) Yuan, X.; Hatch, H. W.; Conrad, J. C.; Marciel, A. B.; Palmer, J. C. pH response of sequence-controlled polyampholyte brushes. *Soft Matter* **2023**, *19*, 4333−4344.
(51) Sanjuan, S.; Tran, Y. Stimuli-Responsive Interfaces Using Random Polyampholyte Brushes. *Macromolecules* **2008**, *41*, 8721−8728.
(52) Jackson, N. E.; Brettmann, B. K.; Vishwanath, V.; Tirrell, M.; de Pablo, J. J. Comparing Solvophobic and Multivalent Induced Collapse in Polyelectrolyte Brushes. *ACS Macro Lett.* **2017**, *6*, 155−160.
(53) Synytska, A.; Biehlig, E.; Ionov, L. Adaptive PEG−PDMS Brushes: Effect of Architecture on Adhesiveness in Air and under Water. *Macromolecules* **2014**, *47*, 8377−8385.
(54) Hou, L.; Wu, P. Comparison of LCST-transitions of homopolymer mixture, diblock and statistical copolymers of NIPAM and VCL in water. *Soft Matter* **2015**, *11*, 2771−2781.
(55) Wang, J.; Müller, M. Microphase Separation of Diblock Copolymer Brushes in Selective Solvents: Single-Chain-in-Mean-Field Simulations and Integral Geometry Analysis. *Macromolecules* **2009**, *42*, 2251−2264.
(56) Chu, E.; Babar, T.; Bruist, M. F.; Sidorenko, A. Binary Polymer Brushes of Strongly Immiscible Polymers. *ACS Appl. Mater. Interfaces* **2015**, *7*, 12505−12515.
(57) Fox, T. L.; Tang, S.; Horton, J. M.; Holdaway, H. A.; Zhao, B.; Zhu, L.; Stewart, P. L. In Situ Characterization of Binary Mixed Polymer Brush-Grafted Silica Nanoparticles in Aqueous and Organic Solvents by Cryo-Electron Tomography. *Langmuir* **2015**, *31*, 8680−8688.
(58) Quan, X.; Peng, C.; Dong, J.; Zhou, J. Structural properties of polymer-brush-grafted gold nanoparticles at the oil−water interface: insights from coarse-grained simulations. *Soft Matter* **2016**, *12*, 3352−3359.
(59) Guo, Y.; Moffitt, M. G. Semiconductor Quantum Dots with Environmentally Responsive Mixed Polystyrene/Poly(methyl methacrylate) Brush Layers. *Macromolecules* **2007**, *40*, 5868−5878.
(60) Li, D.; Sheng, X.; Zhao, B. Environmentally Responsive "Hairy" Nanoparticles:□ Mixed Homopolymer Brushes on Silica Nanoparticles Synthesized by Living Radical Polymerization Techniques. *J. Am. Chem. Soc.* **2005**, *127*, 6248−6256.
(61) Smith, J. D.; Chen, R.; Osores, N. N.; Gopalan, P. Porous Morphology of High Grafting Density Mixed Polyelectrolyte Brushes Grown from a Y-Inimer Coating. *Langmuir* **2024**, *40*, 10623−10633.
(62) Huang, X.; Hauptmann, N.; Appelhans, D.; Formanek, P.; Frank, S.; Kaskel, S.; Temme, A.; Voit, B. Synthesis of Hetero-Polymer Functionalized Nanocarriers by Combining Surface-Initiated ATRP and RAFT Polymerization. *Small* **2012**, *8*, 3579−3583.
(63) Nagase, K.; Wakayama, H.; Matsuda, J.; Kojima, N.; Kanazawa, H. Thermoresponsive mixed polymer brush to effectively control the adhesion and separation of stem cells by altering temperature. *Mater. Today Bio* **2023**, *20*, 100627.
(64) Zhao, B.; Brittain, W. J. Synthesis, Characterization, and Properties of Tethered Polystyrene-b-polyacrylate Brushes on Flat Silicate Substrates. *Macromolecules* **2000**, *33*, 8813−8820.
(65) Xu, C.; Wu, T.; Drain, C. M.; Batteas, J. D.; Fasolka, M. J.; Beers, K. L. Effect of Block Length on Solvent Response of Block Copolymer Brushes:□ Combinatorial Study with Block Copolymer Brush Gradients. *Macromolecules* **2006**, *39*, 3359−3364.
(66) Ayres, N.; Boyes, S. G.; Brittain, W. J. Stimuli-Responsive Polyelectrolyte Polymer Brushes Prepared via Atom-Transfer Radical Polymerization. *Langmuir* **2007**, *23*, 182−189.
(67) Bütün, V.; Armes, S. P.; Billingham, N. C. Selective Quaternization of 2-(Dimethylamino)ethyl Methacrylate Residues in Tertiary Amine Methacrylate Diblock Copolymers. *Macromolecules* **2001**, *34*, 1148−1159.
(68) Sanjuan, S.; Perrin, P.; Pantoustier, N.; Tran, Y. Synthesis and Swelling Behavior of pH-Responsive Polybase Brushes. *Langmuir* **2007**, *23*, 5769−5778.
(69) Toomey, R.; Tirrell, M. Functional Polymer Brushes in Aqueous Media from Self-Assembled and Surface-Initiated Polymers. *Annu. Rev. Phys. Chem.* **2008**, *59*, 493−517.
(70) Qu, F.; Li, D.; Ma, X.; Chen, F.; Gautrot, J. E. A Kinetic Model of Oligonucleotide−Brush Interactions for the Rational Design of Gene Delivery Vectors. *Biomacromolecules* **2019**, *20*, 2218−2229.
(71) Galvin, C. J.; Genzer, J. Swelling of Hydrophilic Polymer Brushes by Water and Alcohol Vapors. *Macromolecules* **2016**, *49*, 4316−4329.
(72) Deodhar, C.; Soto-Cantu, E.; Uhrig, D.; Bonnesen, P.; Lokitz, B. S.; Ankner, J. F.; Kilbey, S. M. I. Hydration in Weak Polyelectrolyte Brushes. *ACS Macro Lett.* **2013**, *2*, 398−402.
(73) Ko, Y.; Miles, J. R.; Genzer, J. Determining Water Sorption and Desorption in Thin Hydrophilic Polymer Films by Thermal Treatment. *ACS Appl. Polym. Mater.* **2019**, *1*, 2495−2502.
(74) Mandal, J.; Arcifa, A.; Spencer, D. N. Synthesis of acrylamide-based block-copolymer brushes under flow: monitoring real-time growth and surface restructuring upon drying. *Polym. Chem.* **2020**, *11*, 3209−3216.
(75) Takei, Y. G.; Aoki, T.; Sanui, K.; Ogata, N.; Sakurai, Y.; Okano, T. Dynamic Contact Angle Measurement of Temperature-Responsive Surface Properties for Poly(N-isopropylacrylamide) Grafted Surfaces. *Macromolecules* **1994**, *27*, 6163−6166.
(76) Dong, R.; Lindau, M.; Ober, C. K. Dissociation Behavior of Weak Polyelectrolyte Brushes on a Planar Surface. *Langmuir* **2009**, *25*, 4774−4779.
(77) Ko, Y.; Christau, S.; von Klitzing, R.; Genzer, J. Charge Density Gradients of Polymer Thin Film by Gaseous Phase Quaternization. *ACS Macro Lett.* **2020**, *9*, 158−162.
(78) Cheng, N.; Bao, P.; Evans, S. D.; Leggett, G. J.; Armes, S. P. Facile Formation of Highly Mobile Supported Lipid Bilayers on Surface-Quaternized pH-Responsive Polymer Brushes. *Macromolecules* **2015**, *48*, 3095−3103.
(79) Ratner, B. D.; Castner, D. G. *Surface Analysis-The Principal Techniques*; John Wiley & Sons, Ltd, 2009; pp 47−112.
(80) Zhao, R.; Fu, C.; Wang, Z.; Pan, M.; Ma, B.; Yin, Q.; Chen, B.; Liu, J.; Xia, H.; Wan, F.; Wang, L.; Zhang, Q.; Wang, Y. A pH-Responsive Nanoparticle Library with Precise pH Tunability by Co-Polymerization with Non-Ionizable Monomers. *Angew. Chem., Int. Ed.* **2022**, *61*, No. e202200152.
(81) de Gennes, P. G. Conformations of Polymers Attached to an Interface. *Macromolecules* **1980**, *13*, 1069−1075.
(82) Varma, S.; Bureau, L.; Débarre, D. The Conformation of Thermoresponsive Polymer Brushes Probed by Optical Reflectivity. *Langmuir* **2016**, *32*, 3152−3163.
(83) Mondarte, E. A. Q.; Shi, Y.; Koh, X. Q.; Feng, X.; Daniel, D.; Zhang, X.-X.; Yu, J. Unveiling the Layered Structure of Sulfobetaine Polymer Brushes through Bimodal Atomic Force Microscopy. *Macromolecules* **2023**, *56*, 5001−5009.
(84) Horst, R. J.; Brió Pérez, M.; Cohen, R.; Cirelli, M.; Dueñas Robles, P. S.; Elshof, M. G.; Andreski, A.; Hempenius, M. A.; Benes, N. E.; Damen, C.; de Beer, S. Swelling of Poly(methyl acrylate) Brushes in Acetone Vapor. *Langmuir* **2020**, *36*, 12053−12060.
(85) Zhu, B.; Edmondson, S. Polydopamine-melanin initiators for Surface-initiated ATRP. *Polymer* **2011**, *52*, 2141−2149.